On the Optimal Paper Moebius Band

Richard Evan Schwartz *

December 22, 2024

Abstract

There are two main conjectures about paper Moebius bands. First, a smooth embedded paper Moebius band must have aspect ratio at least $\sqrt{3}$. Second, any sequence of smooth embedded paper Moebius bands having aspect ratio converging to $\sqrt{3}$ converges, in the Hausdorff topology and up to isometries, to an equilateral triangle of semi-perimeter $\sqrt{3}$. We will reduce these conjectures to 10 statements about the positivity of certain explicit piecewise algebraic expressions.

1 Introduction

An embedded (respectively immersed) *paper Moebius band* of aspect ratio λ is a smooth isometric embedding (respectively immersion) $I : M_\lambda \to \boldsymbol{R}^3$, where M_λ is the flat Mobius band

$$M_\lambda = ([0,1] \times [0,\lambda])/\sim, \qquad (x,0) \sim (1-x,\lambda) \tag{1}$$

Let λ_0 be the infimal value of λ such that there exists a smooth embedded paper Moebius band of aspect ratio λ. Halpern and Weaver [**HW**] prove that $\lambda_0 \in [\pi/2, \sqrt{3}]$.

Halpern and Weaver make the following conjecture about λ_0.

Conjecture 1.1 (Optimality) *A smooth embedded paper Moebius band has aspect ratio greater than $\sqrt{3}$. Hence $\lambda_0 = \sqrt{3}$.*

*Supported by N.S.F. Grant DMS-1807320

Here is an elaboration on the Optimality Conjecture:

Conjecture 1.2 (Rigidity) *A sequence of smooth embedded paper Mobius bands having aspect ratio converging to $\sqrt{3}$ converges, in the Hausdorff metric and up to isometries, to an equilateral triangle of semi-perimeter $\sqrt{3}$.*

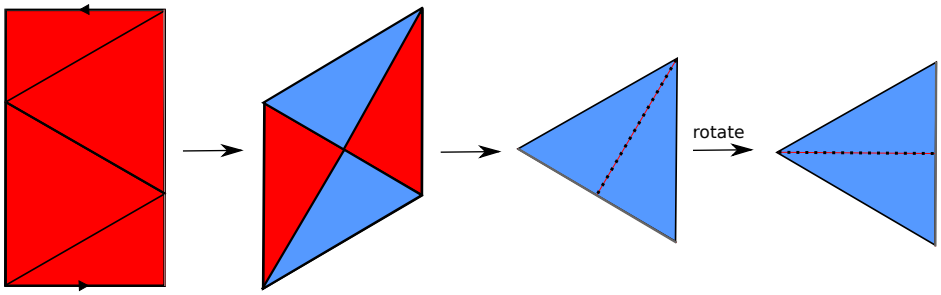

Figure 1.1: The presumed optimizer

Figure 1.1 shows the concrete construction which realizes the equilateral triangle of semi-perimeter $\sqrt{3}$ as the limit of a sequence of embedded paper Moebius bands. The Rigidity Conjecture is really saying that this is the only possibility. In [**S1**] we improve the lower bound to $\lambda_0 \geq \lambda_1$, where λ_1 is some explicit algebraic number greater than $\sqrt{3} - (1/26)$. In [**S2**] we prove additional geometric estimates related to this.

In this paper, which is a sequel to [**S1**] and [**S2**], we will reduce the Optimality and Rigidity Conjectures to a ten purely geometric estimates about certain finite graphs. A paper Moebius bend behaves somewhat like a tensegrity [**CB**]. It is ruled by a continuous family of line segments which, individually, are completely rigid like the bars in a tensegrity. The directions transverse to the bend lines are like the cables of a tensegrity; they are drawn together by the spatial embedding. By remembering just a finite number of bends, we can approximate a paper Moebius band by a finite graphs which have these kinds of properties. It is tempting to call our graphs tensegrities, but our treatment of them differs in some ways from the way tensegrities are usually treated. So, instead, we call these graphs *ladders*.

In §2, after recalling some notions and results from [**S1**] and [**S2**], I prove the Optimality Theorem and the Rigidity Theorem modulo two main results, the Geometry Lemma and the Topology Lemma. The Geometry Lemma also works in the immersed case (with a side condition concerning something called a T-pattern) and the Topology Lemma requires an embedding.

In §3 I discuss the ladders we use in the calculations. I also discuss what I call the *capacity* of a ladder. The capacity of a given ladder serves as a lower bound to the aspect ratio of the corresponding paper Moebius band which it approximates.

In §4 I reduce the Topology Lemma to 5 calculations involving the capacity of ladders. The Topology Lemma is a very natural statement which possibly has a more traditional proof.

In §5 I reduce the Geometry Lemma to 5 more ladder capacity calculations.

In §6 I discuss the extent to which I have verified the computations numerically. The basic idea is that I don't see any counter-examples when I run numerical optimization algorithms on the relevant quantities. I have posted my computer code on my website:

http://www.math.brown.edu/∼res/Java/MOEBIUS.tar.

The interested reader can also run the calculations, tweaking the parameters in various ways.

I want to emphasize that I have not rigorously established the 10 calculations which go into the proofs of the Topology and Geometry Lemma. I am very confident about the 5 that go into the Topology Lemma and somewhat less confident about the 5 that go into the Geometry Lemma. Needless to say, I will withdraw or revise this paper if I find counter-examples to any of the calculations.

I would like to thank Bob Connelly, Dan Cristofaro-Gardiner, Dmitry Fuchs, Steven D. Miller, and Sergei Tabachnikov for helpful discussions about this problem. I would especially like to thank Sergei for telling me about the problem and pointing me to his book with Dmitry. I would also like to acknowledge the support of the Simons Foundation, in the form of a 2020-21 Simons Sabbatical Fellowship, and also the support of the Institute for Advanced Study, in the form of a 2020-21 membership funded by a grant from the Ambrose Monell Foundation.

2 The Proof modulo Two Lemmas

In this chapter we recall some concepts and results from [**S1**] and then reduce the two main theorems to two auxiliary lemmas, the Geometry Lemma and the Topology Lemma.

2.1 Polygonal Moebius Bands

Say that a *polygonal Moebius band* is a pair $\mathcal{M} = (\lambda, I)$ where $I : M_\lambda \to \boldsymbol{R}^3$ is a continuous mapping that is an isometry on each triangle of a triangulation of M_λ. We insist that the vertices of these triangles all lie on ∂M_λ, as in Figure 1.1. In [**S1**, §4] explain how the results we got about polygonal Moebius bands imply the results in the smooth case. The same remarks apply here. We henceforth work entirely with polygonal Moebius bands.

A *bend* is a line segment which has its endpoints on ∂M_λ and lies entirely within one of the triangles of the triangulation. The Moebius band M_λ has a continuous foliation by bends. A *bend image* is a segment of the form $I(\beta)$, where β is a bend. In the smooth case, the bend images are the ruling lines of the ruled surface. A *T-pattern* is a pair of perpendicular coplanar bend images with disjoint interiors. Figures 1.1 and 2.1 show examples. In [**S1**] we prove the following result.

Lemma 2.1 *A polygonal Moebius band of aspect ratio less than* $7\pi/12$ *has a T-pattern.*

The T-pattern in our polygonal Moebius band may not be unique, but we fix a T-pattern once and for all. Let β_1 and β_2 be two bends whose corresponding images $\beta_1^* = I(\beta_1)$ and $\beta_2^* = I(\beta_2)$ form a T-pattern. We call these the *special bends*. Since the segments β_1^* and β_2^* have disjoint interiors, we can label so that the line extending β_2^* does not intersect the interior of β_1^*. The results in [**S2**] show that this labeling is unique: The line extending β_1^* does intersect β_2^*, and in a point within $1/30$ of the midpoint of β_2^*.

We cut M_λ open along β_1 and treat β_1 as the bottom edge. We now label β_1 and β_2 respectively by B and T, which also serve as the lengths of these segments. We normalize so that $I(B)$ connects $(-B, 0, 0)$ to $(0, 0, 0)$, and $I(T)$ is a translate, in the XY-plane of the segment connecting $(0, 0, 0)$ to $(0, T, 0)$. See Figure 2.1.

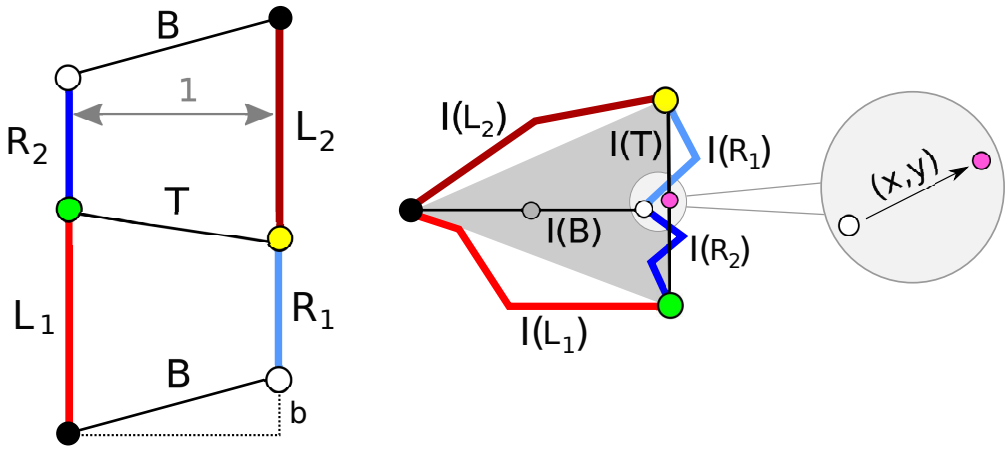

Figure 2.1: The standard normalization

The left side of Figure 2.1 shows M_λ. Reflecting in a vertical line, we normalize so that $L_1 \geq R_1$. This means that $L_2 \geq R_2$. We set

$$S_j = L_j + R_j. \tag{2}$$

We call this the *standard normalization*. The trapezoids τ_1 and τ_2 are the closures of $M_\lambda - (T \cup B)$. The pair (τ_1, τ_2) will be a frequent companion for us during the paper.

The middle part of Figure 2.1 shows the T pattern, and the corresponding images of the sets on the left under the isometry I. The wiggly curves we have drawn do not necessarily lie in the XY-plane but their endpoints do. We normalize so thatIn the figure (x, y) denotes the vector which points from the white to the pink vertex on the right side. We have blown this part of the figure up to make it more visible. The right part of Figure 2.1 is a close-up of a feature of the middle part of the picture.

Remark: Actually, there are two standard normalizations. We can make the replacements $M_\lambda \to \rho_1(M_\lambda)$ and $I \to \rho_2 \circ I \circ \rho_1$, where ρ_1 is reflection in the midpoint of M_λ and ρ_2 is reflection in the X-axis. This change preserves all our normalizations, and gives us a similar picture with a trapezoid isometric to τ_1 stacked above a trapezoid isometric to τ_2. The new vector (x, y) changes to $(x, -y)$. This trick lets us interchange the roles of the indices in various arguments. So, if we prove a certain statement for (τ_1, τ_2) then we get the same result for (τ_2, τ_1).

2.2 Important Bends

Numerical experiments motivate the definitions I give here, which otherwise might seem fairly unmotivated.

Pitch: Given a polygonal Moebius band with a T-pattern, we use the standard normalization. For each bend β we let $\beta^* = \pi \circ I(\beta)$, the projection of the bend image $I(\beta)$ into the XY-plane. Each bend β of τ_1 has associated to it an angle $\theta \in [0, \pi]$ such that when we rotate the positive X-axis counterclockwise by θ we arrive at a ray parallel to β^*. We call θ the *pitch*. We always take the pitch to lie in $[-\pi/2, 3\pi/2]$.

Four Bends: Let $(k)_1$ stand for a bend β of τ_1 whose bend pitch is $+k\pi/12$. Let $(k)_2$ stand for a bend β of τ_2 whose bend pitch is $\pi - k\pi/12$. We insist that $(0)_1 = (0)_2 = (0)$ is the bottom bend and $(6)_1 = (6)_2 = (6)$ is the top. We are interested in bends $(0), (1)_j, (4)_j, (6)$ for $j = 1, 2$. We pick $(1)_j$ and $(4)_j$ to be the bends nearest (0) and (6), respectively, which satisfy the conditions. Let π be projection into the XY-plane. We illustrate our notation by example:

$$(4)_1^* = \pi \circ I((4)_1) \tag{3}$$

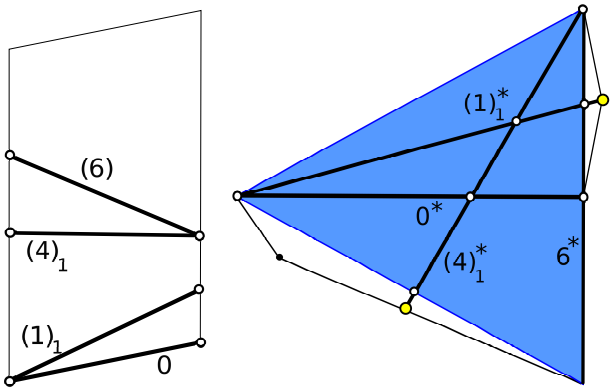

Figure 2.2: The 4 important bends and the yellow tips.

Ranges of Bends: We define our notation by way of example. Let the interval $[0, 1]_1$ denote all the bends in the trapezoid τ_1 that interpolate between 0 and 1_1. As another example $[4, 6]_2$ denotes all the bends in the trapezoid τ_2 which interpolate between 4_2 and 6_2.

Tips: We define the 1-*tip* of τ_j^* to be the right endpoint of $(1)_j^*$. We define the 4-tip of τ_j to be the left endpoint of $(4)_j^*$. These are the yellow vertices in Figure 2.2. The blue triangle in Figure 2.2 is the convex hull of the T-pattern.

- We write $\tau_i \to_1 \tau_j$ if there is some bend $\beta \in [4,6]_i$ such that β^* contains the 1-tip of τ_j^*.
- We write $\tau_i \to_4 \tau_{3-i}$ if there is some bend $\beta \in [0,4]_i$ such that β^* contains the 4-tip of τ_{3-i}^*.

2.3 The Two Main Lemmas

Henceforth, we set $\sqrt{3}^* = \sqrt{3}+10^{-100}$. The addition of 10^{-100} is an arbitrary but convenient choice. The point here is that, for the Rigidity Theorem, we need to consider aspect ratios slightly larger than $\sqrt{3}$. Here is the main topological component of the proof.

Lemma 2.2 (Topology) *Suppose that (τ_1, τ_2) is a trapezoid pair corresponding to an embedded polygonal Moebius band of aspect ratio less than the quantity $\sqrt{3}^*$. Then at least one of 4 things is true.*

$$\tau_1 \to_1 \tau_1, \qquad \tau_2 \to_1 \tau_1, \qquad \tau_1 \to_4 \tau_2, \qquad \tau_2 \to_4 \tau_1.$$

Lemma 2.3 (Geometry) *Suppose that (τ_1, τ_2) is a trapezoid pair corresponding to an immersed polygonal Moebius band of aspect ratio less than $\sqrt{3}^*$. Suppose also the the Moebius band has a T-pattern. Then the following is true:*

1. *If $\tau_2 \to_4 \tau_1$ then $S_1 + S_2 \geq 2\sqrt{3}$.*
2. *If $\tau_1 \to_1 \tau_1$ then $S_1 \geq \sqrt{3}$.*
3. *If $\tau_1 \to_1 \tau_2$ and $\tau_2 \to_1 \tau_1$ then $S_1 + S_2 \geq 2\sqrt{3}$.*
4. *If $\tau_1 \to_1 \tau_1$ and $\tau_1 \to_1 \tau_2$ then $S_1 + S_2 \geq 2\sqrt{3}$.*

Moreover, for any $\epsilon > 0$ there is a $\delta > 0$ such that if we have equality within δ in any of the cases, then $(0)^* \cup (6)^*$ is within ϵ of an equilateral triangle of perimeter $2\sqrt{3}$ in the Hausdorff metric.

Remark: The Geometry Lemma is a symmetric result. Switching the roles of the indices, we get the same result when $\tau_2 \to_1 \tau_2$, etc. Thus, any of 8 hypotheses lead to the conclusion in the Geometry Lemma.

2.4 Proofs of the Main Results

Proof of the Optimality Theorem: Suppose that $\mathcal{M}$ is an embedded polygonal Moebius band of aspect ratio less than $\sqrt{3}$. Let (τ_1, τ_2) be the associated trapezoid pair, as in Figure 2.1. We have $S_1 + S_2 < 2\sqrt{3}$. We can order so that $S_2 < \sqrt{3}$. From the Geometry Lemma, it is impossible that $\tau_2 \to \tau_2$.

The Topology Lemma, applied to the pair (τ_2, τ_1), leaves 3 possibilities:

1. $\tau_1 \to_4 \tau_2$.
2. $\tau_2 \to_4 \tau_1$.
3. $\tau_1 \to_4 \tau_2$.

The Geometry Lemma rules out Cases 1 and 2.

Consider Case 3. Suppose $\tau_1 \to \tau_2$. Given the cases we have already ruled out, the the Topology Lemma applied to (τ_1, τ_2) tells us that, additionally, either $\tau_1 \to \tau_1$ or $\tau_2 \to \tau_1$. The Geometry Lemma now rules out these two cases. ♠

Proof of the Rigidity Theorem: Suppose we have a sequence of Paper Moebius bands whose aspect ratios converge to $\sqrt{3}$. We can assume that the aspect ratios are all less than $\sqrt{3}^*$. The Topology and Geometry Lemmas apply to all these examples. let us consider what happens as we move through our sequence. By the Geometry Lemma, the convex hull Δ of the T pattern converges (modulo global isometries of $\boldsymbol{R}^3$) to the equilateral triangle Δ_0 of semi-perimeter $\sqrt{3}$. Since the length of the boundary $I(\partial M_\lambda)$ is at least as long as the perimeter of Δ, we see that this boundary must in fact converge in the Hausdorff Topology (modulo global isometries) to this same triangle Δ_0. This proves the Rigidity Theorem. ♠

3 Tensegrities

3.1 Signed Trapezoids and Capacities

Signed Segments: Given a segment $S \subset \boldsymbol{R}^3$ let $|S|$ denote the length of S. We say that a *signed segment* is a pair (S, σ) where $|S| \geq 1$ and $\sigma \in \{-1, 0, 1\}$. If $|S| = 1$ we insist that $\sigma = 0$. if $|S| > 1$ we insist that $\sigma \neq 0$. We say that a *realization* of (S, σ) is a segment $S' \subset \boldsymbol{R}^2$ whose endpoints respectively lie on the lines $x = 0$ and $x = 1$, such that

$$|S'| = |S|, \qquad \sigma\sigma' \geq 0,$$

Here σ' is the slope of S'. There is a 1-parameter family of segments S' realizing S, and they are all vertical translates of each other.

Capacity: Now we define a somewhat fancier invariant. We call Q a *signed quadrilateral* if T and B are signed segments. We say that a *realization* of Q is a trapezoid $Q' = (L', R', T', B')$ such that

- L' lies in the line $x = 0$ and $|L'| \geq |L|$. The left vertex of L' is $(0, 0)$.
- R' lies in the line $x = 1$ and $|R'| \geq |R|$.
- B' realizes B and T' realizes T.
- B' lies beneath T'.

All the different realizations differ from each other by translating R' vertically up and down, and there is some minimal choice of Q' realizing Q. We define

$$\kappa(Q) = |L'| + |R'|, \tag{4}$$

where L' and R' come from the minimal realization. Let b' and t' respectively denote the slopes of B' and T'. We let $d = b' - t'$. Then

$$\kappa(Q) = \max(2|L| - d, 2|R| + d). \tag{5}$$

3.2 Stacked Ladders

Now we consider compound graphs made from concatenating several quadrilaterals together. The word "stacked" comes from the idea that the realization of these graphs will be a vertical stack of trapezoids. The quadrilaterals

comprising the graphs in $\boldsymbol{R}^3$ are not really stacked in this way. Geometrically, they kind of rotate around, like a discrete paper Moebius band.

Abutting Quadrilaterals: Let $Q_j = (L_j, R_j, T_j, B_j)$ be a signed quadrilateral for $j = 1, 2$. We write $Q_1 \to Q_2$ if

- $T_1 = B_2$, as signed segments.
- $T_1 \cap L_1 = B_2 \cap L_2$ and $T_1 \cap R_1 = B_2 \cap R_2$.

We write $Q_1 \rightsquigarrow Q_2$ if

- $T_1 = B_2$, as signed segments.
- $T_1 \cap R_1 = B_2 \cap L_2$ and $T_1 \cap L_1 = B_2 \cap R_2$.

Main Definition: We say that a *stacked ladder of complexity* N is a list $Q_1 \to ... \to Q_N$ of signed quadrilaterals. We call the ladder *cyclic* if, additionally, we have $Q_n \rightsquigarrow Q_1$. A cyclic ladder is supposed to be an approximation of a paper Moebius band, as we will see below.

Capacity: Let $\mathcal{Q}$ be a stacked ladder of length N.

$$\kappa(\mathcal{Q}) = \sum_{i=1}^{N} \kappa(Q_i). \tag{6}$$

Capacity of Families: Given some collection $\mathcal{A}$ of ladders, we define $\kappa(\mathcal{A})$ to be the minimum value of κ taken over all members of $\mathcal{A}$. Our families will be such that that κ always achieves its minimum on $\mathcal{A}$. For the Geometry Lemma, (it seems that) there is a unique member of $\mathcal{A}$ on which κ achieves its minimum value. This minimal ladder corresponds to the paper Moebius band depicted in Figure 1.1, the target of the Rigidity Theorem.

3.3 Pitch Specifications

Given a segment $S \subset \boldsymbol{R}^3$ let $\theta(S)$ denote the angle that $\pi(S)$ makes with the X-axis. Here π is projection to the XY-plane. We call $\theta(S)$ the *pitch* of S.

A cyclic stacked ladder of complexity N is determined by the signed segments $B_1, ..., B_N$. We say that an *angle interval* is an interval of the form

$$\Theta = [\theta_1, \theta_2] \subset (-\pi/2, 3\pi/2).$$

We allow $\theta_1 = \theta_2 = \theta$, and in this case we write $\theta = [\theta, \theta]$.

Given N angle intervals Θ_j for $j = 1, ..., n$ we consider the family

$$\mathcal{A}(\Theta_1, ..., \Theta_N)$$

consists of all the ladders such that $\theta(B_k) \in \Theta_k$ for $k = 1, ..., M$. We single out a special index $j > 1$ and place the following constraints:

1. $\Theta_1 = 0$ and the sign of B_1 is 0 or +1.
2. $\Theta_j = \pi/2$ and the sign of B_j is -1.
3. B_1 and B_j are as in Figure 2.1, with $B_1 = I(B)$ and $B_j = I(T)$.

The segments B_1 and B_j play the role of the T-pattern. The sign constraints come from [**S2**, Theorem 3.1], a result which gives us these signs when the paper Moebius band has aspect ratio less than $\sqrt{3}$. Even in the Rigidity Lemma, when we need to consider paper Moebius bands of slightly larger aspect ratio, we can reduce to this case. We explain this in §6. In §6 we will also discuss some further constraints we get from the results in [**S1**] and [**S2**], but these extra constraints are purely for the sake of getting a tidier calculation. They are not essential.

We do not specify the signs for B_k when $k \neq \{1, j\}$. Thus, the family $\mathcal{A}(\cdots)$ typically has 2^{N-2} components, one per sign choice. In almost all cases, there will be some "obvious" component which contains the configurations of lowest capacity. Our program tries all possibilities and finds this best component in an automatic way.

We make all the same definitions for stacked ladders which are not cyclic. In this case we also have to specify a pitch interval and the sign for T_N. In practice, the non-cyclic stacked ladders we consider will be obtained from cyclic stacked ladders simply by forgetting the last quadrilateral.

3.4 Connection to Paper Moebius Bands

Here is the connection to polygonal Moebius bands. Suppose that

$$I : M_\lambda \to \boldsymbol{R}^3$$

is a polygonal Moebius band with a T-pattern. We first cut M_λ open along the special bends as in Figure 2.1. Now suppose that we have a finite list

$\beta_0, ..., \beta_N$ of bends, with β_0 being the bottom and β_N being the top. In Figure 2.1 both β_0 and β_N correspond to bends labeled B. We get a cyclic stacked ladder of complexity N by defining $Q_1, .., Q_N$ as follows:

$$B_k = I(\beta_{k-1}), \qquad T_k = I(\beta_k). \tag{7}$$

L_k connects the endpoints of the curve $I(L_k')$ where L_k' is the segment in the left edge of M_λ whose endpoints are in β_{k-1} and β_k. We make the same definition for R_k with *right* replacing *left*. The signs are determined by the slopes of the bends in the paper Moebius band.

By construction, the trapezoid

$$Q_k' = (L_k', R_k', \beta_k, \beta_{k-1})$$

is a realization for Q_k. Hence

$$2\lambda \geq \kappa(\mathcal{Q}). \tag{8}$$

If we can show that $\mathcal{Q}$ must lie in a certain family of stacked ladders, then a lower bound on κ on this entire family gives a lower bound on λ. This is the strategy we take for the Topology and Geometry Lemmas.

Now we do an example calculation which shows the kinds of conclusions we can draw from the ladder calculations. I have not done this calculation rigorously, but I have experimented with it extensively. Consider the family

$$\mathcal{A}(0, \pi/6, \pi/2).$$

The right side of Figure 3.1 shows an example of a member of $\mathcal{A}$. This member has capacity about $\sqrt{3} - .018$. The left side of Figure 3.1 shows the minimial realization of this ladder. The sign choice is $(+, +, -)$.

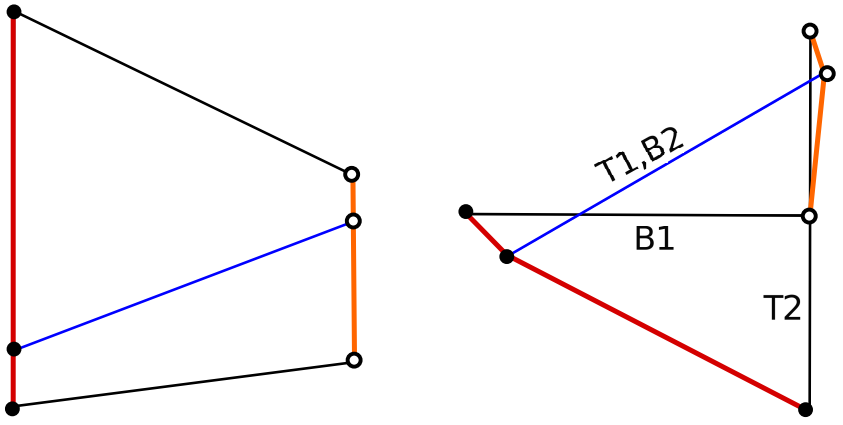

Figure 3.1: A member of $\mathcal{A}$ and its minimal realization.

We notice experimentally that for all $\mathcal{Q} \in \mathcal{A}$ we have $\kappa(\mathcal{Q}) > \sqrt{3} - \frac{1}{50}$. Let us consider the implication of this calculation. The left side of Figure 3.1 involves the bottom trapezoid in Figure 2.1. If our calculation is really correct, it implies that

$$S_1 = L_1 + R_1 > \sqrt{3} - \frac{1}{50}.$$

But then, interchanging the roles of the indices, we get the same result for S_2. Hence

$$2\lambda = S_1 + S_2 > 2\sqrt{3} + \frac{1}{25}.$$

This yields

$$\lambda > \sqrt{3} - \frac{1}{50}.$$

This is an improvement on the bound from [**S1**], which states that $\lambda > \lambda_1$, where λ_1 is very close to $\sqrt{3} - \frac{1}{26}$.

Remark:
You could replace the pitch $\pi/6$ with some other angle θ, and this would yield a different infimum $\kappa(\theta)$ over all ladders in the corresponding families. After quite a bit of experimentation, I think that the choice $\theta = \pi/6$ gives the best answer. That is, $\kappa(\theta) \leq \kappa(\pi/6)$.

3.5 Crossing Penalties

The Penalty Function: Let V_1, V_2, V_3, V_4 be 4 vectors, with $V_j = (V_{j1}, V_{j2}, V_{j3})$.

$$(i, j) = \det(V_1, V_2) = V_{11}V_{22} - V_{12}V_{21}. \tag{9}$$

When $k \geq 3$ we define

$$(i_1, ..., i_k) = (i_1, i_2) + ... + (i_{k-1}, i_k) + (i_k, i_1). \tag{10}$$

The following function χ is positive if and only if V_1V_2 and V_3V_4 cross at a point, interior to both segments, when projected into the XY plane.

$$\chi = \frac{2}{(1,4,2,3)} \max(0, \min((1,2,3), (1,4,3), (2,1,4), (2,3,4)). \tag{11}$$

We derive the equation in Equation 11 as follows. We solve the equation

$$(1-s)A_1 + sA_2 = (1-t)A_3 + tA_4$$

for s and t. The individual expressions comprising Equation 11, e.g.

$$\frac{(1,2,3)}{(1,4,2,3)},$$

compute $s, t, 1-s, 1-t$, and they are all positive exactly when our two segments cross at points which are interior to both.

Enhanced Capacity: We will use the function χ in the next chapter, as a kind of enhancement of the capacity, when we are interested in ladders where certain segments in $\boldsymbol{R}^3$ are meant to project to disjoint segments in the XY-plane. Modifying the capacity by the crossing penalty function is a trick that will allow us to ignore the cases when the projections cross.

Given a stacked ladder $\mathcal{Q}$ and some pair i, j of indices, we define

$$\kappa(i, j, \mathcal{Q}) = \kappa(\mathcal{Q}) + \mu\chi(B_i, B_j). \tag{12}$$

Here $\mu > 0$. In practice we take $\mu = 128$. The function $\kappa(i, j, *)$ gives a penalty – i.e., it takes on an artificially large value – for $\mathcal{Q}$ in case the segments B_i and B_j project into the plane in such a way as to cross each other. If the segments to not cross, we have $\kappa(i, j, \mathcal{Q}) = \kappa(\mathcal{Q})$.

A Variant: There is also a variant we consider. We define

$$\chi_1 = \frac{2}{(1,4,2,3)} \max(0, \min((1,2,3), (1,4,3), (2,1,4)). \tag{13}$$

In deriving this expression we have omitted the triple which does not involve the index 1. In a similar way, we can define χ_α for $\alpha = 2, 3, 4$. Let us explain the reason why we consider this variant. There are 4 (non-exclusive) ways that two segments in the plane can fail to cross. In all cases, one of the segments lies on one side of the line extending the other segment. The function above vanishes in three of these instances but remains positive for the fourth. We define

$$\kappa(\alpha; i, j, \mathcal{Q}) = \kappa(\mathcal{Q}) + \mu\chi_\alpha(B_i, B_j). \tag{14}$$

Again, we take $\mu = 128$. We will see in the next chapter how we use this variant computationally.

3.6 Modified Capacity

One operation we can do with our graphs is delete or add edges. When we delete edges, we "weaken" the graph and when we add edges we "strengthen" it. For instance, if we remove the signed edges we can define the simpler capacity

$$\kappa_0(Q) = |L| + |R|.$$

We have $\kappa_0 \leq \kappa$. To see the difference, suppose that Q is a degenerate quadrilateral, with $|R| = 0$ and $|L| = |T| = |B| = 1$. Then Q' is a square with side length 1. Hence $\kappa_0(Q) = 1$ and $\kappa(Q) = 2$. More generally, we can introduce the intermediate quantity

$$\kappa_u = (1-u)\kappa_0 + u\kappa. \tag{15}$$

As u ranges in $[0,1]$ this quantity interpolates between κ_0 and κ.

Going in the other direction, we can produce a stronger invariant by also considering the diagonal edges of Q. In our definition of $\kappa(Q)$ above, we use the minimal realization Q' of Q. We say that a realization Q'' of Q is *diagonally good* if each diagonal of Q'' is at least as long as each diagonal of Q. This might or might not happen for Q'. We can define $\widehat{\kappa}(Q) = |L''|+|R''|$, where L'' and R'' are the vertical sides of the minimal realization Q'' that is diagonally good. We have $\kappa(Q) \leq \widehat{\kappa}(Q)$, and our main inequality below, Equation 8, also works with $\widehat{\kappa}$ in place of κ.

4 The Topology Lemma

In this chapter we reduce the Topology Lemma to 5 graph calculations. As in previous chapters $I : M_\lambda \to \boldsymbol{R}^3$ is a polygonal Moebius band of aspect ratio at most $\sqrt{3}^*$. Also $\beta^* = \pi \circ I(\beta)$. We first prove the Topology Lemma under a condition we call *Topological Goodness*. Following this, we reduce topological goodness to a property we call *Geometrical Goodness*, a purely geometric property. We then reduce Geometrical Goodness to 5 ladder calculations.

4.1 Topological Goodness

Given 2 bends β_1 and β_2 we write $\beta_1|\beta_2$ if β_1^* and β_2^* intersect in a point that is interior to both. Assuming that $\beta_1|\beta_2$, we write $\beta_1 \uparrow \beta_2$ if the vertical line through $\beta_1^* \cap \beta_2^*$ intersects $I(\beta_1)$ above where it intersects $I(\beta_2)$. Otherwise we write $\beta_1 \downarrow \beta_2$. We must have one or the other when we have an embedded Moebius band. We will encode the information below in a picture reminiscent of a knot diagram.

We call $(\beta_1, \beta_2, \beta_3)$ a *topologically bad triple* triple if the crossings are inconsistent in one of two ways:

- $\beta_1 \uparrow \beta_2$ and $\beta_1 \downarrow \beta_3$.
- $\beta_1 \downarrow \beta_2$ and $\beta_1 \uparrow \beta_3$.

Otherwise we call the triple *topologically good*.

Good Pairs: We say that the pair (τ_1, τ_2) is *topologically good* if:

1. $(0)|(4)_j$ and $(1)_1|(4)_j$ and $(4)_1|(4)_2$.
2. $(4_j, 1_1, 0)$ is topologically good.
3. $(1_1, 4_j, 6)$ is topologically good unless $\tau_j \to_1 \tau_1$.
4. $(4_{3-j}, 4_j, 0)$ is topologically good unless $\tau_j \to_4 \tau_{3-j}$.

Here $j = 1, 2$ in all statements.

Our next result proves the Topology Lemma under the assumption that we have a topologically good pair. The basic idea is that various topological crossing diagrams are impossible under the assumptions above, and this forces the desired incidences.

Lemma 4.1 *The Topology Lemma holds for topologically good pairs.*

Proof: Suppose first that $(1)_1^*$ and 6^* do not cross. Since $(1)_1|(4)$, there is by continuity some $\beta \in [4,6]_1$ such that β^* contains the 1-tip of $(1)_1^*$. This means that $\tau_1 \to \tau_1$.

Henceforth we assume $(1)_1|(6)$. We normalize by an ambient isometry so that $(1)_1 \downarrow (6)$. Figure 4.1 shows the 4 possibilities.

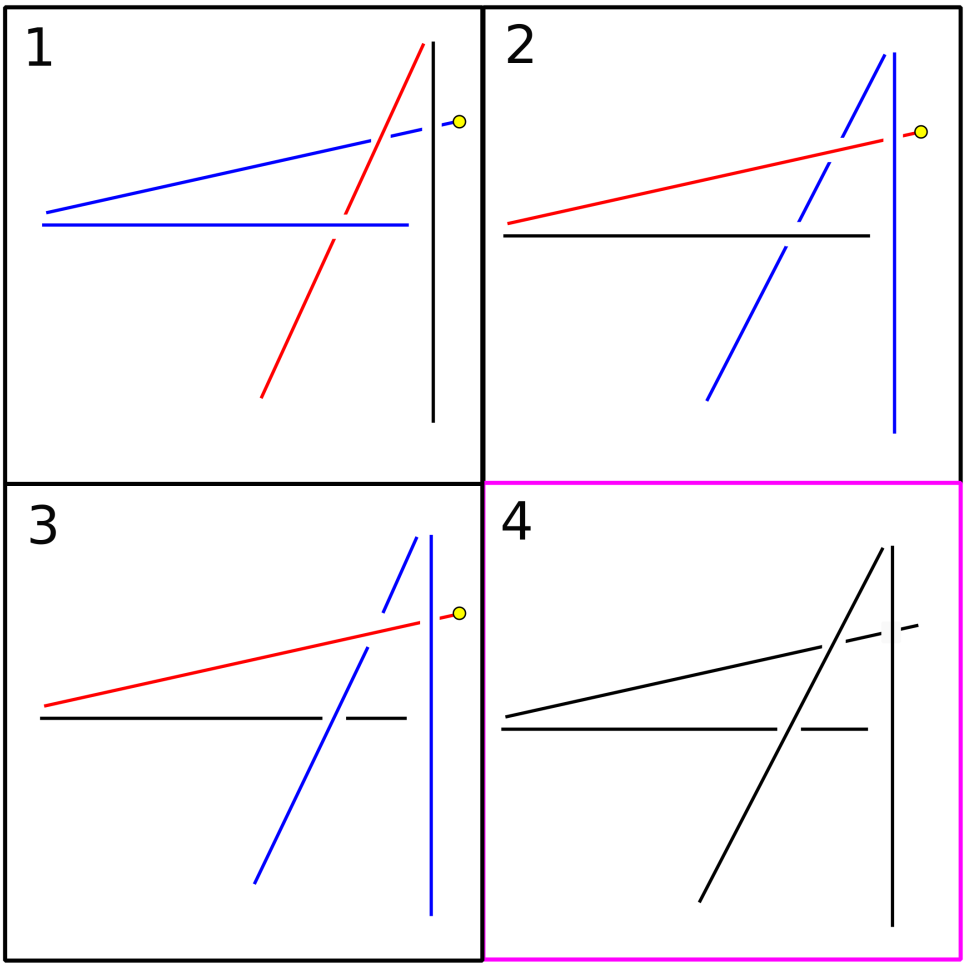

Figure 4.1: Four possibilities

Case 1 has the topologically bad triple $(4_1, 1_1, 0)$, so this case cannot happen. Cases 2 and 3 have the topologically bad triple $(1_1, 4_1, 6)$. Hence $\tau_1 \to_1 \tau_1$ in these cases. This leaves Case 4.

Let us explore Case 4 in more detail. Figure 4.2 shows the situation.

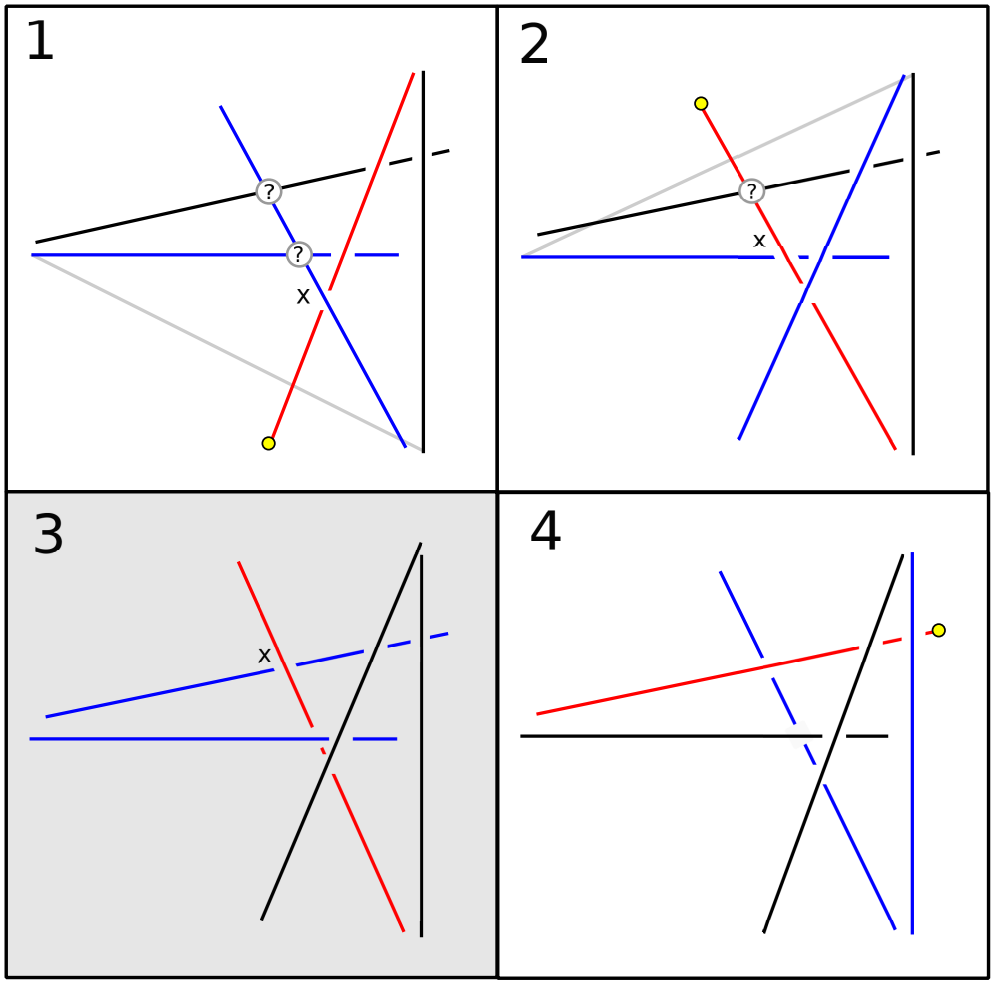

Figure 4.2: Four possibilities

In Case 1 we have left 2 crossings undetermined and we place an x by the crossing we study. If the crossing is as appears, then $(4_1, 4_2, 0)$ is a topologically bad triple. But then $\tau_2 \rightarrow_4 \tau_1$.

In Case 2 we are working on the next crossing, and we still leave one undetermined. This has the same structure as Case 1 but with the indices 1 and 2 reversed. Hence $\tau_1 \rightarrow_4 \tau_2$ here.

In Case 3, the situation is impossible because $(4_2, 1_1, 0)$ is a topologically bad triple.

In Case 4, the triple $(1_1, 4_2, 6)$ is topologically bad. Hence $\tau_2 \rightarrow_1 \tau_1$. ♠

4.2 Geometrical Goodness

Here we give conditions under which the pair (τ_1, τ_2) is topologically good. We call the triple $(\beta_1, \beta_2, \beta_3)$ of bends *geometrically good* if $\beta_1 | \beta$ for all bends β that interpolate between β_2 and β_3. We always work with bends which are confined to one or the other of the trapezoids τ_1, τ_2, so there is no ambiguity about what the word *interpolate* means. In the next result, we have our standard normalization. We call (τ_1, τ_2) *geometrically good* if the various conditions on the triples in the definition of topological goodness hold with the word *geometrically* replacing the word *topologically* in every instance.

Lemma 4.2 *(τ_1, τ_2) is topologically good if (τ_1, τ_2) is geometrically good.*

Proof: For a given triple, the implication "geometric implies topological" works the same way in all cases. We just consider two representative cases.

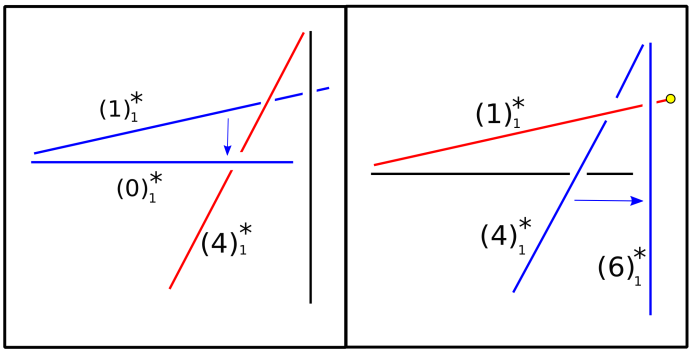

Figure 4.3: A topological contradiction.

First look at the left half of Figure 4.3. Consider the triple $(4_1, 1_1, 0)$. In $\boldsymbol{R}^3$, as we sweep the blue $I(I_1)$ over to the blue $I(0)$ we end up on the wrong side of the red $I(4_1)$. The geometrical goodness prevents the crossing type from changing.

Now look at the right half of Figure 4.3. As we sweep the blue $I(4_1)$ over to the blue $I(6)$, we get the same contradiction as in the previous case, except that now the crossing can change if the projection of one of the blue segments in our sweepout contains the right endpoint of $(1)_1^*$. In other words, $(1_1, 4_1, 6)$ is topologically good unless $\tau_1 \to_1 \tau_1$. ♠

4.3 Pitch Bounds

As a prelude to establishing geometrical goodness, we discuss the range of pitches for some of the bends in our polygonal Moebius band. We keep the notation from above. This next result is proved under the assumption that our polygonal Moebius band has aspect ratio at most $\sqrt{3}^* = \sqrt{3} + 10^{-100}$.

Lemma 4.3 *If $\beta_1, \beta_2, \beta_3$ are 3 bends, appearing in order in one of the two trapezoids associated to the T-pattern, then $\theta(\beta_2)$ is at most $\pi/30$ from the interval bounded by $\theta(\beta_1)$ and $\theta(\beta_2)$.*

Proof: This is Theorem 5.1 in [**S2**]. ♠

Recall that the interval $[0,1]_1$ denote all the bends in the trapezoid τ_1 that interpolate between 0 and 1_1. Let $\Theta([0,1]_1)$ denote the range of bend pitches for bend images in $[0,1]_1$. We make similar definitions for the other intervals.

Lemma 4.4 *Let $\theta_0 = \pi/30$. For any trapezoid pair (τ_1, τ_2) corresponding to a polygonal Moebius band of aspect ratio less than $\sqrt{3} + 10^{-100}$, the following is true:*

1. $\Theta([0,1]_1) \subset [-\theta_0, \pi/12]$.
2. $\Theta([0,4]_1) \subset [-\theta_0, 4\pi/12 + \theta_0]$.
3. $\Theta([4,6]_1) \subset [4\pi/12, \pi/2 + \theta_0]$.

Proof: We just prove the first case. The other cases have the same treatment. It follows immediately from Lemma 4.3 that

$$\Theta([0,1]_1) \subset [-\theta_0, \pi/12 + \theta_0].$$

In other words, we just widen both sides by θ_0. The reason why $\Theta([0,1]_1)$ ends at $\pi/12$ rather than $\pi/12 + \theta$ for some positive θ is that we take $(1)_1$ be the first bend after $(0)_1$ with pitch $\pi/12$. ♠

4.4 Establishing Geometrical Goodness

Let the interval $[a, b]$ stand for $(\pi a/12, \pi b/12)$. We also set $a_\pm = a \pm (2/5)$. This $[0, 4_+]$ represents the interval $[0, \pi/3 + \pi/30]$.

Our ladder calculations, if correct and if done rigorously, would show that the following ladder families have capacity at least $2\sqrt{3}^*$. In each case, we list the capacity function we use. We have written in bold the positions corresponding to the T-pattern.

$$\mathcal{A}(\mathbf{0}, [0_-, 1], 4, \mathbf{6}); \qquad \kappa(2, 3, *). \tag{16}$$

$$\mathcal{A}(\mathbf{0}, [0_-, 1], \mathbf{6}, 8); \qquad \kappa(2, 4, *) \tag{17}$$

$$\mathcal{A}(0, 1, [4, 6_+], \mathbf{6}). \qquad \kappa(4; 2, 3, *). \tag{18}$$

$$\mathcal{A}(\mathbf{0}, 1, \mathbf{6}, [6_-, 8); \qquad \kappa(4; 2, 4, *). \tag{19}$$

$$\mathcal{A}(\mathbf{0}, 4, \mathbf{6}, [8_-, 12]); \qquad \kappa(2; 2, 4, *). \tag{20}$$

In all our results to follow we fix a polygonal Moebius band $\mathcal{M}$ of aspect ratio less than $\sqrt{3}^*$ and we cut it open along the special bends. This gives us our trapezoid pair (τ_1, τ_2) as above. All the statements below are taken with respect to these objects, and *good* means *geometrically good*.

Lemma 4.5 *If Equation 16 is true, then* $(4_1, 1_1, 0)$ *is good.*

Proof: Let π be projection into the XY-plane. Suppose that $(4_1, 1_1, 0)$ is not good. This means that we have a bend $\beta \in [0, 1]_1$ such that β^* and $(4)_1^*$ do not cross. By Lemma 4.4 and our method of approximating $\mathcal{M}$ by a cyclic ladder, we get a member $\mathcal{Q}$ of $\mathcal{A}(...)$, the family in Equation 16, such that the bends $\pi(B_2)$ and $\pi(B_3)$ do not cross. Here $\pi(B_2) = \beta^*$ and $\pi(B_3) = (4_1)^*$. But then we have

$$\kappa(2, 3, \mathcal{Q}) = \kappa(\mathcal{Q}) < 2\sqrt{3}^*.$$

The equality comes from the fact that $\pi(B_2)$ and $\pi(B_3)$ do not cross. The equality comes from Equation 8. Our equation contradicts Equation 16. ♠

Lemma 4.6 *If Equation 17 is true, then* $(4_2, 1_1, 0)$ *is good.*

Proof: This has the same proof as the previous result. ♠

Lemma 4.7 *If Equation 18 is true, then* $(1_1, 4_1, 6)$ *is good unless* $\tau_1 \to_1 \tau_1$.

Proof: The proof is similar to the previous two cases, but we use a modified penalty function. This function is 0 when $\pi(B_2)$ and $\pi(B_3)$ fail to cross, unless $\pi(B_2)$ lies to the left of the line containing $\pi(B_3)$. In this situation we would have $\tau_1 \to_1 \tau_1$. ♠

Lemma 4.8 *If Equation 19 is true, then* $(1_1, 4_2, 6)$ *is good unless* $\tau_2 \to_1 \tau_1$.

Proof: The proof is the same as in the previous case. ♠

Lemma 4.9 *If Equation 20 is true, then* $(4_1, 4_2, 6)$ *is good unless* $\tau_2 \to_4 \tau_1$.

Proof: The proof is the same as in the previous case. ♠

The results for the remaining triples associated to the Topology Lemma follow from the results above and the operation of interchanging the roles of the two indices.

Remark: There is one source of programming error that can creep into Equations 18, 19, and 20. We will discuss this for Equation 18. The considerations are the same for the other two equations. in Equation 18 we chose the index $\alpha = 4$ for the modified penalty function $\chi_{1,\alpha}$. One might worry (as we did) that we have chosen the wrong value of α. The correspondence between indices and cases corresponds to the way we have parametrized the segments, and it is easy to make a mistake when figuring out which index corresponds to which case. Here is how we make sure we have the right choice, namely $\alpha = 4$ in this case. When we use any index α other than 4 in this calculation, the enhanced capacity fairly rapidly converges to a number less than $\sqrt{3}$ and the plot shows the case when $\pi(B_2)$ lies to the left of the line containing $\pi(B_3)$. In other words, the other three choices do not penalize this case. This tells us that the choice $\alpha = 4$ is correct.

5 The Geometry Lemma

5.1 Notation

Our Topology Lemma calculations all used the penalty function to force the computer to consider the case of (certain) non-crossing segments. We could make similar kinds of calculations for the Geometry Lemma, but we are going to take a more efficient approach.

To explain our new approach, we refine the kind of ladder family that we have already considered in the previous chapter. We let

$$\mathcal{A}(\Theta_1, ..., \Theta_N; i_1 \to j_1, ..., i_k \to j_k) \tag{21}$$

denote the subspace of $\mathcal{A}(\Theta_1, ..., \Theta_N)$ in which the planar segment $\pi(B_{j_1})$ contains the right endpoint of the planar segment $\pi(B_{i_1})$, and so on. When we want to specify the left endpoint rather than the right endpoint we will use the symbol $i_1 \leftarrow j_1$, etc. In this situation $\pi(B_{j_1})$ contains the left endpoint of $\pi(B_{i_1})$.

We also mention one other modification. There is one situation in which we will not work with a cyclic stacked ladder but just a stacked ladder. In this case we will use the notation $\mathcal{B}(\cdots)$ instead of $\mathcal{A}(\cdots)$. As we will discuss below, the corresponding $\mathcal{A}$-family does not have the desired properties. Note that when the arguments are the same, the $\mathcal{A}$ family has one more quadrilateral than the $\mathcal{B}$ family. For this reason, the capacities of members of the $\mathcal{B}$ family to be lower than the capacities of the corresponding members of the $\mathcal{A}$ family. We are leaving off the last quadrilateral when we make our sum.

Each of our families below will contain a member $\mathcal{Q}_0$ which comes from approximating the polygonal Moebius band from Figure 1.1. When the family in question is $\mathcal{B}(\cdots)$ we have $\kappa_1(\mathcal{Q}_0) = \sqrt{3}$. When the family in question is $\mathcal{A}(\cdots)$ we have $\kappa_1(\mathcal{Q}) = 2\sqrt{3}$. We call one of these families *good* if we have $\kappa_1(\mathcal{Q}) \geq \kappa_1(\mathcal{Q}_0)$ with equality only if $\mathcal{Q} = \mathcal{Q}_0$. All the calculations we present amount to saying that various ladder families are good. Our families are tailored to match the conditions in the Geometry Lemma. We will have 5 rather than 4 families, because one of the cases splits into two sub-cases.

5.2 The Calculations

The calculations below, if correct and done rigorously, would show that the following ladder families are good. In all cases we use the plain capacity function κ. We use the same notation as in §4.4.

$$\mathcal{A}(\mathbf{0}, 4, \mathbf{6}, [8, 12_+]; 2 \leftarrow 4) \tag{22}$$

$$\mathcal{B}(\mathbf{0}, 1, [4, 6_+], \mathbf{6}; 2 \to 3) \tag{23}$$

$$\mathcal{A}(\mathbf{0}, 1, [4, 6_+], \mathbf{6}, [6_-, 8], 11; 2 \to 5, 6 \to 3) \tag{24}$$

$$\mathcal{A}(\mathbf{0}, 1, [4, 6_+], [6_-, 8], \mathbf{6}, 11; 2 \to 3, 6 \to 4) \tag{25}$$

$$\mathcal{A}(\mathbf{0}, 1, [4, 6_+], [6_-, 8], \mathbf{6}, 11; 2 \to 4, 6 \to 3) \tag{26}$$

These calculations combine in a straightforward way with Lemma 4.4 to establish the Geometry Lemma. The first 3 calculations correspond respectively to Cases 1,2,3 in the Geometry Lemma. The last two cases both correspond to Case 4. Let us explain why there are two cases here. The condition we have is that $\tau_1 \to_1 \tau_2$ and $\tau_1 \to_1 \tau_2$. So, there are two bends $\beta_1, \beta_2 \in [4, 6]_1$, with the following properties:

- β_1^* contains the right tip of $(1)_1^*$.
- β_2^* contains the right tip of $(1)_2^*$.

As we move through $[4, 6]_1$ we have to encounter one or the other of these bends first. We get the two cases above depending on which order we have. The other cases do not have this problem because in the other cases the relevant bend images contain just one bend of interest.

We also note that Calculation 23 is actually a lot more like Calculation 24 then it first first appears. If we "double" this calculation by also considering the symmetric situation in the upper trapezoid τ_2, then we arrive at the family:

$$\mathcal{A}(\mathbf{0}, 1, [4, 6_+], \mathbf{6}, [6_-, 8], 11; 2 \to 3, 6 \to 5) \tag{27}$$

This family differs from the one in Equation 24 just in way that the segments are "linked" at the end. We might have worked with Calculation 27 but in this one case we can do a simpler calculation.

6 Numerical Computations

6.1 Constraints

For the purposes of giving rigorous proofs, it is important that we consider all possible ladders that could arise in the families from Equations 16–20 and Equations 22–26. However, for the purposes of doing numerical experiments to determine whether a rigorous proof ultimately will be possible, it is better to restrict the range of possibilities as much as possible. In this section we explain various ways we limit the range of possibilities we consider, for the purposes of making good numerical experiments.

T Pattern Geometry: Let B_1 and B_j be the segments corresponding to the T-pattern. Referring to Figure 2.1, we have $B_1 = I(B)$ and $B_j = I(T)$. (Here j is the special index discussed in §3.3.) As in Figure 2.1, we normalize so that the right endpoint of of B_1 is the origin and both B_1 and B_j lie in the XY-plane. In [**S2**, Theorem 4.1] we show that when the polygonal Moebius band has aspect ratio less than $\sqrt{3}^*$ we have $x \in [0, 1/18]$ and $|y| < 1/30$. Here (x, y) is as in Figure 2.1. This vector points from the right endpoint of B_1, which is the origin, to the midpoint of B_j.

Spatial Displacement: We constrain the third coordinates of our ladders to lie in the interval $[-1/2, 1/2]$. Remember that we are normalizing so that the T-pattern lies in the XY-plane. If any vertex has large Z-coordinate this adds quite a bit to the capacity. We have not yet formally justified this constraint, but it seems quite reasonable for the purposes of experimentation.

Center Constraints: When there are no other constraints on a center of a signed segment, we constrain it so that each coordinate of the center is within $1/2$ of the corresponding center for the member corresponding to the example in Figure 1.1. Again, we did not formally justify this constraint, but the same considerations as for the spacial displacement constraints would apply here.

Angle Constraints: Recall that B_1 and B_j are signed segments. The signs indicate the signs of the slopes b and t of the segments marked B and T on the left side of Figure 2.1. In [**S2**] we prove that when the capacity of the polygonal Moebius band is less than $\sqrt{3}$ the point (b, t) lies in the blue

region shown in Figure 6.2. Since this blue region is rather complicated to describe, we show in [**S2**] that it lies inside the indicated trapezoid.

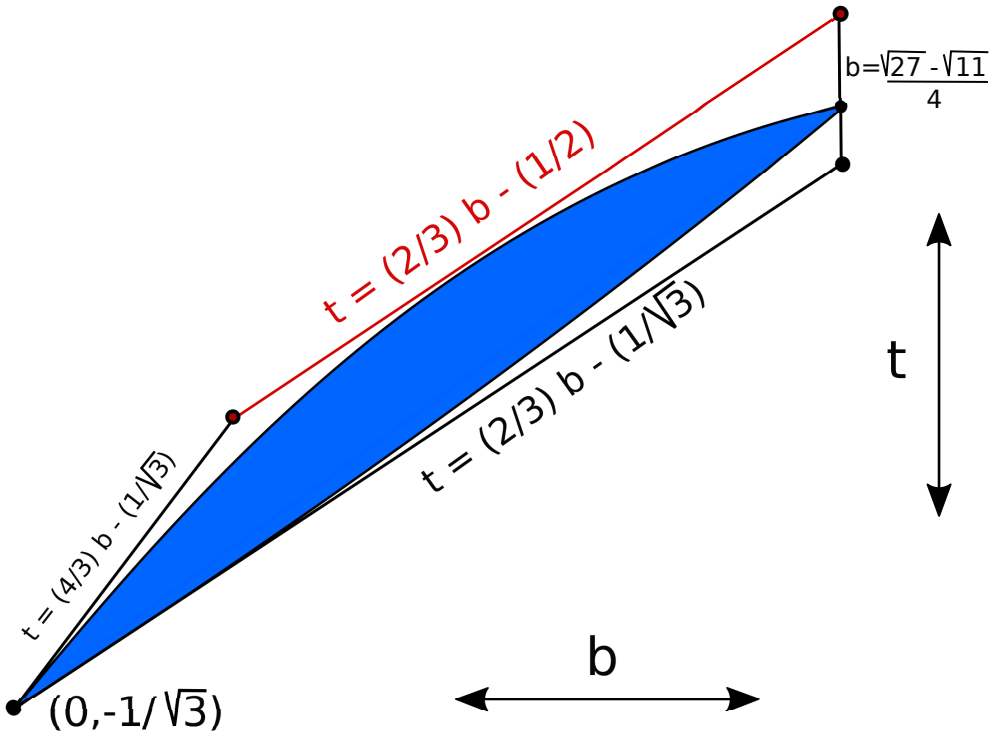

Figure 6.2: The confining trapezoid

These constraints in turn place constraints on the maximum length of the segments B_1 and B_j. They also force the sign of B_1 to 0 or positive and the sign of B_j to be negative.

It is worth noting that, since we are considering polygonal Moebius bands of aspect ratio less than $\sqrt{3}^*$ rather than $\sqrt{3}$, we do have to deal with the possibility that B_1 has negative sign. However, given a sequence of examples of paper Moebius bands whose aspect ratio converges to $\sqrt{3}$, the pair $\{(b_n, t_n)\}$ either converges (on a subsequence) to the point $(0, 1/\sqrt{3})$ or it does not. In the first case, convex hull of the T-pattern converges to a triangle whose base is $2/\sqrt{3}$ and whose height is 1. Such a triangle has perimeter at least $\sqrt{3}$, and so the Rigidity Theorem holds for such a sequence. In the other case, the segment B_1 eventually has positive sign. In short, we do not lose generality by forcing the sign of B_1 to be 0 or positive.

6.2 Parametrizing Ladders

We arrange that a point in $[0,1]^K$ corresponds to a ladder in one of our families. We have $K = 16$ for all the families in Equations 16–20, and we have $K = 14, 14, 24, 24, 24$ for the families in Equations 22–26 respectively.

When the family has $L + 2$ signed segments, we split our cube into a product $[0,1]^K = [0,1]^{K-2L} \times [0,1]^{2L}$. The $2L$ variables at the end specify the third coordinates of the signed segments which are not part of the T-pattern. Each coordinate h in $[0,1]^{2L}$ specifies the height $h - 1/2$ for one of the endpoints of the signed segments. To describe what we do with the parameters in $[0,1]^{K-2L}$ we introduce the function

$$I(a,b,r) = (1-r)a + rb. \tag{28}$$

This function maps $[0,1]$ onto $[a,b]$. Here is how we use a point

$$(r_1, ..., r_{K-2L}) \in [0,1]^{K-2L},$$

and also an auxiliary choice of signs

$$(\sigma_1, ..., \sigma_L) \in \{-1, 1\}^L.$$

- **T-Pattern Geometry:** The first two variables (r_1, r_2) specify the signed segments which participate in the I-pattern. We set

  $$b = I(0, \beta, r_1), \qquad t = I(b_-, b_+, r_2), \qquad \beta = (\sqrt{27} - \sqrt{11})/4.$$

  Here $y = b_-, b_+$ are the endpoints of the intersection of the line $x = b$ with the trapezoid in Figure 6.2. The pair (b,t) in turn specifies the lengths and signs of the signed segments B_1 and B_j which participate in the T-pattern. The variables (r_3, r_4) specify the vector (x,y) considered above, as follows:

  $$x = I(0, 1/18, r_2), \qquad y = I(-1/30, 1/30, r_4).$$

- **The Pitches:** The next string of variables specify the pitches of the signed segments. The ranges are determined by the arguments in the family. For instance, for the family in Equation 23 we have $L = 1$ and the pitch of B_2 is specified by

  $$I\left(\frac{4\pi}{12}, \frac{6\pi}{12} + \frac{\pi}{30}, r_5\right).$$

- **Lengths:** The next string of variables specify the lengths of the signed segments other than B_1 and B_j, the ones participating in the T-pattern.

- **Centers:** The remaining variables specify the centers of the signed segments. When there are no other constraints, each coordinate r gives a value $I(-1,1,r)$ for one of the coordinates of one of the centers. When we need to enforce some extra constraints, we use a single variable r to specify the center of a given signed segment. For the family in Equation 22, we pick the center of B_4 in such a way that $\pi(B_4)$ contains the left endpoint ℓ of $\pi(B_2)$. Suppose we use the variable r for this purpose. Then the case $r = 0$ forces one endpoint of $\pi(B_4)$ to equal ℓ and the case $r = 1$ forces this for the other endpoint. As r ranges in $[0,1]$ we interpolate between these two extreme cases. Thus we need only one variable for the centers. The other constraints, for the other families, are treated similarly.

- **Signs:** We use the point $\sigma \in \{-1,1\}^L$ to specify the signs of the signed segments which do not participate in the T-pattern. We never specify a sign of 0 because our calculations are just numerical and the case of a signed segment (of length 1) and sign 0 is a boundary case.

There are two other features of our parametrization we mention. First, we notice experimentally that the presumed minimizers in all families appear to have all the spatial variables equal to 0. When we allow the spatial variables to range freely, the our numerical optimization algorithm decreases the value of the capacity much more slowly. (We have no proof of this.) When we want to find the minimum fast, we set the spatial variables equal to zero.

Second, in the case of the families in Equations 22–26, where we suspect that the capacity minimizer corresponds to the equilateral example in Figure 1.1, we have a mechanism for focusing the calculation around this point. In each family, there is a variable choice $r_0 \in [0,1]^K$ corresponding to the equilateral example. We can set a parameter $u \geq 0$ and then consider the following transformation

$$r \to \frac{r + ur_0}{1+u}. \tag{29}$$

When $u = 0$ this transformation is the identity. As u increases, the transformation carries r increasingly close to r_0. So, if we want to focus our attention around the presumed minimizer, we take some nonzero u when we run the calculations. I call u the *coercion factor*.

6.3 Numerical Optimization

We have our capacity function $f : X \to \boldsymbol{R}_+$. Here $X = [0,1]^K \times \{-1,1\}^L$. For the families in Equations 22–26 we have $f = \kappa$, the basic function. For the families in Equations 16–20, we have $f = \kappa + \chi$, where χ is the relevant crossing penalty function. Our computer program allows us to consider the more general function $\kappa + \mu\chi$ for any positive multiple μ. The larger we take μ, the more we force the computer to ignore the cases when the segments of interest to us cross. If we can show that $\min f > 2\sqrt{3}$ for any choice of μ, we get the desired result, so there is no reason why we cannot choose μ as large as we like. We take $\mu = 128$ in our calculations below.

Here we describe a basic numerical optimization algorithm called [1] *hill climbing*. Given $r \in \boldsymbol{R}$ we define $[r]$ to be the closest point in $[0,1]$ to r. Given a vector $\mathbf{r}$ we define $[\mathbf{r}]$ to be the result of applying $[\cdot]$ coordinatewise. We start with some initial point $r_0 \in X$ We pick a small random step size s and a random point $r_1 \in [-1,1]^K$. We then replace r_0 by

$$[(1-s)r_0 + sr_1]$$

In other words, we take a small step in a random direction and then retract to X if necessary. If $f(r_1) < f(r_0)$ we replace r_0 with r_1 and repeat.

The hill-climbing algorithm produces a sequence of points $r_0, r_1, r_2, ...$ on which f is decreasing. The hope is that this sequence converges to a global minimum. This algorithm is a reasonable approximation to Newton's method. At least at points where κ is smooth, a small step in a random direction has a 50 percent change of moving in the direction of the gradient. and a somewhat lower but still decent chance of making a small angle with the gradient. Our program lets you adjust the (average) step size to taste.

One trouble with the algorithm is that point sequences can get stuck in local minima which are not global minima. Another trouble, related more directly to our specific application, is that the proceedure keeps us in the same component of X. In other words, the sign choices do not change. To remedy this situation, we introduce a parameter $T > 0$, the *refresh time*. As soon as our algorithm has run for T units of time, we start with an initial guess. Typically, we take T to be 1 second. This refresh option allows us to make a different sign choice and start again. When T is small the algorithm is close to random sampling. When T is large the algorithn is close to hill-climbing. My program lets you choose T to taste.

[1] Actually, in the case at hand, the name *hill descending* would be more apt.

6.4 Topology Lemma Calculations

The calculation for the family in Equation 16 is fairly delicate, and the calculations for the families in Equations 17–20 are fairly robust. For the families in equations 17–20 the minimum seems to be larger than $2\sqrt{3} + .1$.

The calculation in Equation 16 is delicate. After running the program for about 6 hours with a refresh time of 1 second and a coercion factor of 32 we get a minimum value of about $2\sqrt{3} + .03$. In this calculation, we set all the spatial variables equal to 0 and used the preferred sign choice. When we leave the spatial variables free, the convergence to a minimum seems to be much slower. Figure 6.3 shows a ladder from the family whose capacity is about $2\sqrt{3} + .05$. The left side of the picture shows the signed segments and the right side shows the signed and unsigned segments together.

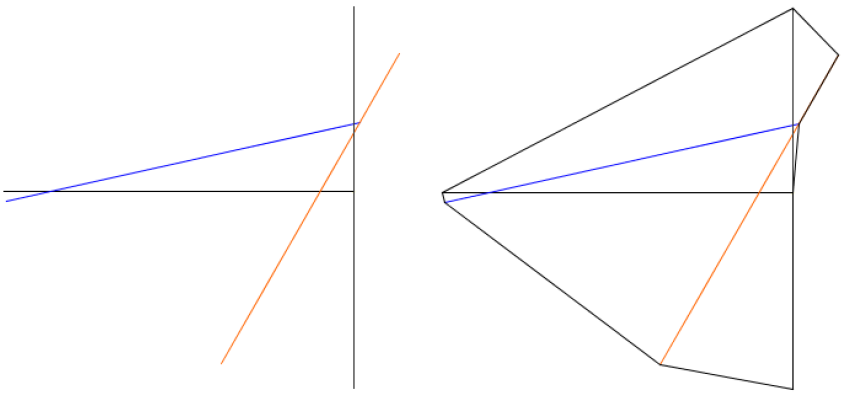

Figure 6.3: A configuration in $\mathcal{A}(\mathbf{0}, [0_-, 1], 4, \mathbf{6})$ having low capacity.

Here is another way to indicate the delicate nature of the calculation. We can find values less than $2\sqrt{3}$ when we run the calculation on the slightly modified family

$$\mathcal{A}(\mathbf{0}, [0_-, 1_+], 4, \mathbf{6}); \qquad \kappa(2, 3, *). \tag{30}$$

Just allowing the blue segment in Figure 6.3 to increase its angle with the X-axis by another $\pi/30$ units causes the calculation to go bad.

One way to get a more robust calculation would be to use the invariant $\widehat{\kappa}$, defined in §3.6, in place of κ. I did try this yet for the specific calculation above, but for related calculations (which were precursors to the ones here) I found that the calculations were much more robust.

6.5 An Alternate Approach

Before coming up with the Topology Lemma calculations discussed above, I had another approach. This other approach is more complicated but The alternate approach involves calculations which are lower dimensional. Rather than having 16-dimensional calculations we can get away with many 10-dimensional calculations and two 14-dimensional calculations.

Say that a *prism* is the set of the form $C \times \boldsymbol{R}$ where C is a convex planar polygon. Say that a *prism pair* is a pair of two disjoint prisms. Say that a prism pair *confines* a line segment if one endpoint of the segment lies in one prism and the other endpoint lies in the other. Say that two prisms P_1 and P_2 are *interlaced* if the following is true. If P_k confines σ_k for $k = 1, 2$ then the projections of σ_1 and σ_2 into the plane cross each other.

The idea of the alternate calculations is to show that the various pairs of segments of interest to use are confined by interlaced prism pairs. The corresponding calculations are all 10 dimensional. The point is that we can treat one of our two segments at a time when establishing the confining property. The interlacing property is then a separate property which we see just by inspection. This method very nearly works. There are two cases where we need to do something more involved, like the calculations above. The interested reader can see these calculations in action using our computer program.

6.6 Geometry Lemma Calculations

I have done many experiments with these calculations. Let describe the strongest recent ones. Given a complexity N stacked ladder $\mathcal{Q}$ and a vector $\mathbf{u} \in [0,1]^N$ we define

$$\kappa_{\mathbf{u}}(\mathcal{Q}) = \sum_{i=1}^{N} \kappa_{u_i}(Q_i). \tag{31}$$

When $\mathbf{u} = (1, ..., 1)$ we recover the original notion of capacity. We call u a *mask*. The function $\kappa_{\mathbf{u}}$ is monotone increasing with each coordinate of $\mathbf{u}$. See §3.6.

After running the program for 6 hours, with the same parameters as above, first with a 1 second refresh time and then with an 8 second refresh time, I found that the capacities remain above $2\sqrt{3}$ when I use the following masks respectively:

1. $(a, a, 0, 0)$.
2. $(a, a, 0)$.
3. $(0, a, 0, 0, a, 0)$.
4. $(a, a, 0, 0, a, 0)$.
5. $(a, a, 0, 0, a, 0)$.

Here $a = .36$. I want to emphasize that if all these capacities stay above $2\sqrt{3}$ then so does the original capacity. So, the numerical results just described are stronger than the test of the basic quantities.

6.7 Some Controls

Here are some examples of related calculations which did not work out. These calculations serve as some controls that the computer program is operating reasonably. The reader can try all these failed calculations using my comoputer program.

First, the families in Equations 22, 25, 26 respectively are not good with respect to the masks $(0, 1, 0, 0)$, $(0, 1, 0, 0, 1, 0)$ and $(0, 1, 0, 0, 1, 0)$.

Second, the related family

$$\mathcal{A}(\mathbf{0}, 1, [4, 6_+], \mathbf{6}; 2 \to 3) \tag{32}$$

is not good. This is the same as the family in Equation 23 except that we are adding in the last quadrilateral (corresponding to τ_2 in Figure 2.1.) It turns out that this family has some ladders of capacity less than $2\sqrt{3}$. My intuition behind this problem is that the family in Equation 32 is a strict relaxation of the family in Equation 27. Put another way, we get the family in Equation 27 by adding constraints to the family in Equation 32.

In place of Calculations 24–26 we originally tried the single family

$$\mathcal{A}(\mathbf{0}, 1, [4, 6_+], \mathbf{6}, 11; 6 \to 3) \tag{33}$$

Were this family good, it would take care of Cases 3 and 4 of the Geometry Lemma at the same time. We get this family from considering the polygonal Moebius bands in which $\tau_1 \to_1 \tau_2$. Unfortunately, the family in Equation 33 also has ladders with capacity less than $2\sqrt{3}$. My intuition behind this is that the families in Equation 32 and 33 are about as "strong" as each other, and neither is "strong enough".

7 References

[**AHLM**] A. Malaga, S. Lelievre, E. Harriss, P. Arnoux, *ICERM website*: https://im.icerm.brown.edu/portfolio/paper-flat-tori/ (2019)

[**CB**], R. Connolly, A Back, *Mathematics and Tensegrity*, in **American Scientist**, Vol 82 **2**, (March-April 1998) pp 142-151.

[**CF**] Y. Chen and E. Fried, *Mobius bands, unstretchable material sheets and developable surfaces*, Proceedings of the Royal Society A, (2016)

[**CKS**] J. Cantarella, R. Kusner, J. Sullivan, *On the minimum ropelength of knots and links*, Invent. Math. **150** (2) pp 257-286 (2003)

[**FT**], D. Fuchs, S. Tabachnikov, *Mathematical Omnibus: Thirty Lectures on Classic Mathematics*, AMS 2007

[**GS**] G. Schwarz, *A pretender to the title "canonical Moebius strip"*, Pacific J. of Math., **143** (1) pp. 195-200, (1990)

[**HF**, D.F. Hinz, E. Fried, *Translation of Michael Sadowsky's paper 'An elementary proof for the existence of a developable MÖBIUS band and the attribution of the geometric problem to a variational problem'*. J. Elast. 119, 3–6 (2015)

[**HW**], B. Halpern and C. Weaver, *Inverting a cylinder through isometric immersions and embeddings*, Trans. Am. Math. Soc **230**, pp 41.70 (1977)

[**MK**] L. Mahadevan and J. B. Keller, *The shape of a Mobius band*, Proceedings of the Royal Society A (1993)

[**Sa**], M. Sadowski, *Ein elementarer Beweis für die Existenz eines abwickelbaren MÖBIUSschen Bandes und die Zurückführung des geometrischen Problems auf einVariationsproblem*. Sitzungsberichte der Preussischen Akad. der Wissenschaften, physikalisch-mathematische Klasse 22, 412–415.2 (1930)

[**S1**] R. E. Schwartz, *An improved bound on the optimal paper Moebius band*, preprint, 2020

[**S2**] R. E. Schwartz, *Paper Moebius Bands with T Patterns*, preprint, 2020

[**W**] S. Wolfram, *The Mathematica Book, 4th Edition*, Wolfram Media and Cambridge University Press (1999).